

ANALYSES OF UO₂ RIA-TESTS WITH THE CODE TESPA-ROD

H.G. Sonnenburg

*Gesellschaft für Anlagen- und Reaktorsicherheit (GRS),
85748 Garching, Forschungsgelände, Germany*

ABSTRACT

RIA tests from three different test facilities (CABRI, BIGR, NSRR) have been analyzed with the fuel rod code TESPA-ROD. The RIA tests from different test facilities differ in many aspects. In particular the power pulse width varies among these test facilities from 2 ms up to 75 ms. Although the timing of the investigated RIA transients varies and also the coolant surrounding the test rod is different, it is found that all investigated test cases can be well predicted with the TESPA-ROD code when applying a pellet strain model which has been calibrated on the CABRI RepNa2 test.

Because the TESPA-ROD code does not apply a fission gas bubble expansion model which might predict the fuel expansion during the RIA transient, a calibrated pellet strain model is applied instead. This model effectively quantifies the effect of fuel strain which occurs additionally to the thermal related fuel strain. It turns out that all experimental findings on residual cladding strain can be well predicted by this model approach. Furthermore, test cases with failed rods show a rather close agreement between model prediction and experimental finding concerning the fuel rod failure enthalpy.

1. TESPA-ROD MODEL DESCRIPTION

The TESPA-ROD code predicts the behaviour of the fuel rod for both LOCA (loss of coolant accident) and RIA (reactivity initiated accident) transients [SON 07]. It provides a radial description of fuel rod parameters. The parameter prediction of TESPA-ROD is restricted to an axial position of the fuel rod. The axial power factor at this axial position f_z provides the physical relation to the overall fuel rod parameters. (see fig. 1).

Several fuel rod gas compartments are represented by a lumped parameter approach. Distinction is made for fuel rod gap volume, fuel crack volume, fuel rod plenum and fuel dishing and fuel pores. This approach avoids a full 2- or 3-dimensional representation of the fuel rod, but allows the prediction of the fuel rod internal gas pressure.

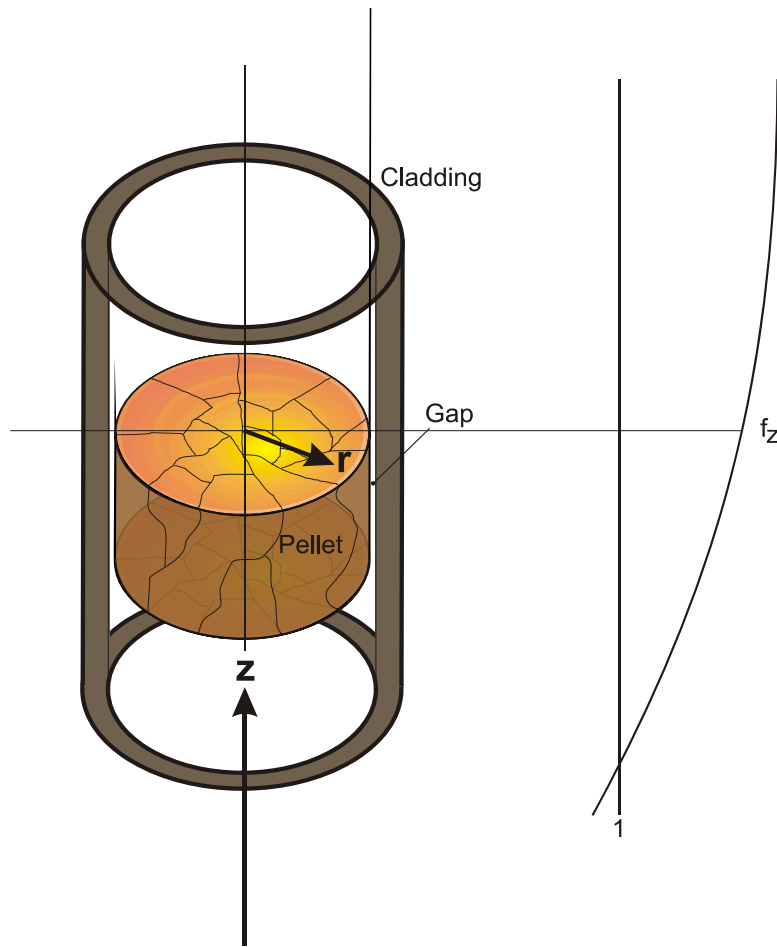


Fig. 1. Axial position under consideration

1.1. Fuel Pellet

The fuel pellet relocation due to pellet cracking is modelled as function of power and burn-up. The empirical model of FRAPCON has been applied for the prediction of this relocation. The swelling of the fuel pellet is modelled with respect to burn-up.

The thermal expansion of the pellet is modelled in TESP-ROD in accordance to the MATPRO 11 correlation. The thermal expansion of the fuel is dependent on the fuel temperature only. Burn-up does not affect this thermal expansion. The linear thermal expansion of the UO₂ pellet material is calculated according to equation (1) with parameters from table 1. This expansion is related to the temperature of 300K:

$$\left. \frac{\Delta L}{L} \right|_{\text{thermic}} = c_1 T - c_2 + c_3 e^{-\frac{E_d}{kT}} \tag{1}$$

Table 1: Parameters for equation (1)

| Parameter [Dimension] | Value |
|--------------------------|------------------------|
| c1 [1/K] | 1 10 ⁻⁵ |
| c2 [-] | 3 10 ⁻³ |
| c3 [-] | 4 10 ⁻² |
| E _d [J] | 6.9 10 ⁻²⁰ |
| k [J/K] | 1.38 10 ⁻²³ |

Melting of the fuel provides an extra thermal strain. The thermal expansion due to melting is modelled according to the MATPRO 11 correlation. If the fuel temperature exceeds the solidus temperature of the fuel, additional strain from the melting process is considered in the TESP-ROD code. If the energy injection leads to melting of the fuel, the latent heat of melting reduces the further temperature increase. Consequently, the thermal strain of the pellet due to melting contributes relatively small to the overall pellet strain when analysing RIA transients.

The effect of fission gas bubble expansion on the pellet straining is not modelled in TESP-ROD. The consideration of this effect will be discussed later in the context of a power density related pellet straining.

The radial power distribution in the pellet is approximated with 10 equidistant nodes. Each node represents a concentric ring of the pellet. The outermost ring is attributed to the rim zone. Depending on burn-up the outermost ring receives an increased power density relative to the remaining rings. The power reduction in the nodes from 1 to 9 is calculated by the empirical equation (2). In order to conserve the energy balance for the entire pellet, the 10th ring receives the energy reduction from the inner rings.

$$x_A = 1 - \frac{Bu \text{ [MWd/kg]}}{300 \text{ MWd/kg}} \quad (2)$$

1.2. Cladding

The material properties of different cladding materials (Zry-4, M5, E110, ...) have been modelled in the code TESP-ROD. The code evaluates the circumferential stress-strain relation only. For the purpose of analysing RIA transients, a strong focus has to be put on the determination of this stress-strain relation, in order to limit the impact from this modelling aspect on the overall calculation uncertainty. Because the pellet exerts a 3-dimensional stress-strain field on the cladding during the RIA transient, the code's circumferential stress-strain relation is determined from the 3-dimensional stress-strain plasticisation theory. In particular this plasticisation theory provides parameters for the yielding of the cladding.

A plain strain condition is assumed within this theory. That is, the axial straining ϵ_{zz} of the cladding due to a tight pellet cladding contact is neglected. Furthermore, shear stresses due

to rotation are assumed not to occur. These assumptions lead to relation between the circumferential stress at yielding and the circumferential stress at burst as stated in equation (3). Relation (3) is valid for ideal plastic behaviour of the cladding.

$$\frac{\sigma_{\text{start of yield}}}{\sigma_{\text{burst}}} = \frac{1}{2} \frac{b^2 - a^2}{b^2 \ln\left(\frac{b}{a}\right)} \dots\dots\dots(3)$$

$$\epsilon_{\text{pl}} = \left[\frac{\sigma_{\text{total}}}{E} \left(\frac{E}{\sigma_{\text{yield}}} \right)^{n-1} \right]^{\frac{1}{n}} - \frac{\sigma_{\text{total}}}{E} \quad \epsilon_{\text{pl}} \geq 0$$

$$\epsilon_{\text{total}} = \left(\frac{\sigma_{\text{total}}}{K} \right)^{\frac{1}{n}} \Leftrightarrow \sigma_{\text{total}} > \sigma_{\text{yield}} = \frac{1}{2} \frac{b^2 - a^2}{b^2 \ln\left(\frac{b}{a}\right)} \sigma_{\text{burst}} \quad (4)$$

$$\epsilon_{\text{el}} = \epsilon_{\text{total}} - \epsilon_{\text{pl}}$$

The stress-strain relation in TESP-ROD is determined from equation (4). The strain hardening exponent n in (4) is estimated to n=0.05 which is suitable for the range of cladding temperatures in RIA transients. The circumferential burst stress σ_{burst} is calculated according to the KfK burst stress model [ERB 80].

If the hydrogen content η in the cladding exceeds 500 ppm, the cladding material is considered as brittle, thus the burst stress and yield stress may have almost same values. The ratio of these values is expected to be 0.985, see equation (5).

$$\sigma_{\text{yield}} = \begin{cases} \frac{1}{2} \frac{b^2 - a^2}{b^2 \ln\left(\frac{b}{a}\right)} \sigma_{\text{burst}} \Leftrightarrow \eta < 500 \text{ ppmH} \\ 0.985 \sigma_{\text{burst}} \Leftrightarrow \eta > 500 \text{ ppmH} \end{cases} \quad (5)$$

The cladding behaviour for both ductile and brittle is schematically shown in fig. 2. It is assumed that the brittle-ductile threshold does not change during the very fast RIA transient.

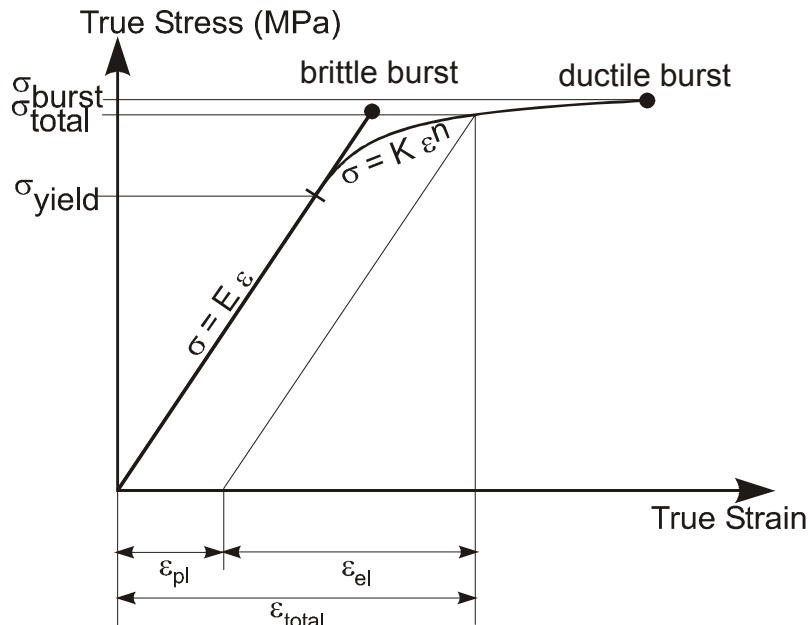


Fig. 2: Stress-strain relation for both ductile and brittle cladding behavior.

For completeness, the Young's modulus E applied in TESPА-ROD is given by:

$$E = \text{MAX}\left(108.8 \text{ GPa} - 0.05475 \frac{\text{GPa}}{\text{K}} T, 40.46 \text{ GPa}\right) \quad (6)$$

2. POST-TEST ANALYSES OF CABRI UO₂ TESTS

2.1. The calibration of a fuel expansion model

The CABRI UO₂ tests, [PAP 03], [PAP 06], with non-failed test rods (RepNa 2, 3, 4, 5, CIP01 and CIP02) have been analyzed with the TESPА-ROD code. These code analyses ignore the extra fuel strain which might result from a fission gas bubble expansion. E.g., the TESPА-ROD post-test predictions for RepNa 2 and 3 are shown in figure 3.

The post-test prediction of the residual cladding strain along different axial positions of the test rod reveals a significant under-prediction of the measured residual strain if the injected energy in the fuel exceeds 110 cal/g. Above 110 cal/g a significant extra fuel strain above the thermal strain takes place.

Residual Strain along Axial Position of Cladding (%)

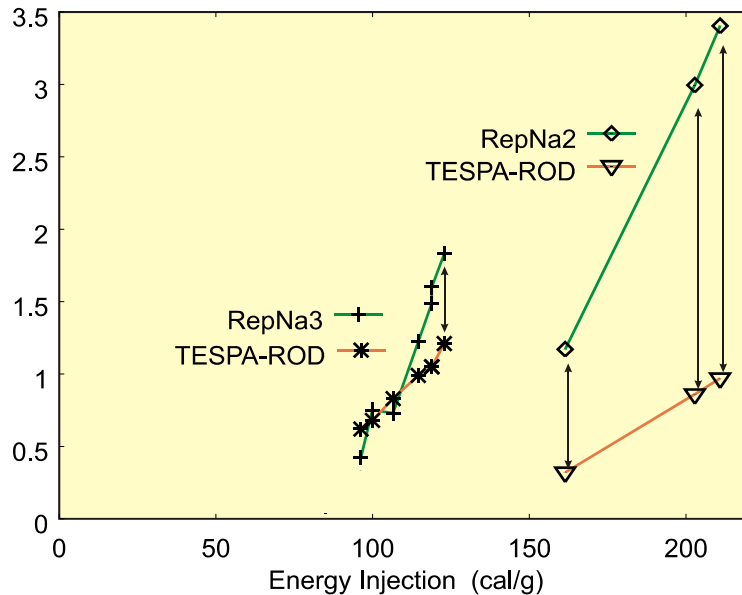


Fig. 3. Comparison of TESP-ROD post-test prediction for CABRI tests RepNa 2 and 3

From a sensitivity study with TESP-ROD it became obvious that modified stress-strain relations, who might enhance the plastic capability of the cladding, cannot improve this severe under-prediction. Finally, the study led to the conclusion that the modeling of the pellet behavior alone can help to improve this situation.

Because the effect of expanding micro bubbles in the fuel matrix is not considered in the code so far, several attempts have been made to identify the correlating fuel parameter which is responsible for the residual cladding strain. Parameters like fuel temperature, fuel burn-up and others have been investigated. It turned out that none of the commonly expected fuel parameters can be considered as a correlating parameter. But when using the local power density of the fuel as a correlating parameter, a very strong correlation for the residual cladding strain could be reached.

This correlation suggests that the fuel straining with power density might be a ceramic process provoked by an extreme high density of atomistic dislocations in the fuel grain. It weakens the strength of the fuel grain and by that allows the micro bubbles inside the grain to expand or the lattice length of the fuel crystals might expand.

The production of dislocations has been estimated for a power density of 700 W/mm^3 to be about $5 \cdot 10^{20}$ Frenkel pairs/ $\text{mm}^3 \cdot \text{s}$. If the pairs produced do not recombine within 10 ms a density of about $5 \cdot 10^{18}$ Frenkel pairs/ mm^3 could be reached. From the literature [OLA 76] a value of 10^{19} Frenkel pairs/ mm^3 is known to generate an amorphous crystal which would explain the weakening of the UO_2 fuel grain.

The CABRI RepNa2 test data alone have been taken in order to quantify the straining of the fuel as function of the power density. The resulting power density correlation is equation (7):

$$\frac{dL}{L} = \frac{dL}{L} \Big|_{\text{thermic}} + 2.8 * 10^{-29} \left(\dot{q}''' \right)^{2.3} \quad (7)$$

Here is \dot{q}''' in W/m^3

The application of correlation (7) in the TESPА-ROD code leads to a remarkable agreement between measured and predicted residual cladding strains for all non-failed claddings of the CABRI UO2 test series (RepNa tests 2, 3, 4 and 5). This agreement is reached for all burn-up levels investigated (RepNa2: 33 MWd/kg; RepNa3: 53 MWd/kg; etc.). There is an excellent prediction for the peak power position of the fuel rod as well as for positions of the fuel rod of less power, see fig. 4.

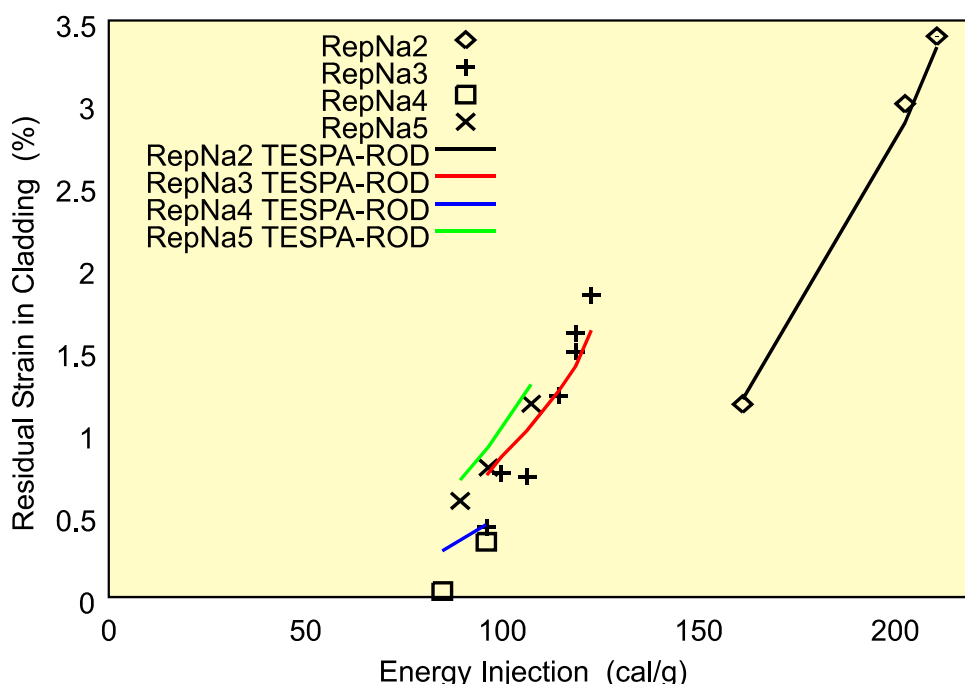


Fig. 4. Comparison for CABRI UO2 tests RepNa 2, 3, 4, 5

The application of correlation (7) suggests that the complex process of the fuel grain weakening and the inter- and intra-granular micro bubble expansion of a fuel grain can be empirically quantified by a single equation. Furthermore, it is surprising that the burn-up and by that the content of fission gas in the grain does not influence this complex process. Otherwise the correlation (7) would need to incorporate certain burn-up dependencies.

2.2. Failed test rods

The claddings of the different test rods of the CABRI UO2 tests have been classified in brittle and ductile according to the hydrogen limit of 500 ppm. According to this limit the test rods of RepNa1, RepNa4, RepNa8, RepNa10 and CIP0-1 are considered as brittle while the remaining test rods are considered as ductile.

Three CABRI UO₂ tests are available which show a burst of the cladding, CABRI RepNa 1, 8 and 10. The burn-up exceeds 60 MWd/kg. The hydrogen content of the three claddings is far beyond 500 ppm which suggests a brittle cladding behavior. The RepNa1 test even shows partial spalling of the oxide layer. The locally spalled oxide increases the hydrogen content much above 1000 ppm.

Table 2: Enthalpy at burst

| Test case | Measurement [cal/g] | Prediction [cal/g] |
|-----------|---------------------|--------------------|
| RepNa 1 | 30 | 42.1 |
| RepNa 4 | - | 83.7 |
| RepNa 8 | 82 | 82.9 |
| RepNa 10 | 79 | 80.3 |

The resulting post-test predictions with the TESP-ROD code for the failure enthalpy are compiled in table 2. Table 2 illustrates, that the predicted fuel enthalpy at burst of the cladding is rather close to the measured enthalpy at burst. Exceptions have to be made for both the CABRI RepNa1 test and the RepNa4 test. The predicted value at burst is 42.1 cal/g for RepNa1 while the measured value is about 30 cal/g. The CABRI RepNa1 test indicates an early failure of the cladding which might be related to the extra hydrogen up-take of the cladding due to the spalled oxide.

The cladding of the test case RepNa4 is considered as brittle because of its high hydrogen content. The TESP-ROD code predicts a fuel rod failure in this case. Further analyses showed that the predicted fuel rod burst stress is rather close to the maximum load achieved during the test transient. Thus, if e.g. the yield-burst stress ratio is slightly shifted from 0.985 to 0.98 this fuel rod can survive the maximum load as non-failed rod. The resulting residual strain reaches a value of 0.44% which is slightly above the measured value of 0.4%.

3. PREDICTION OF SELECTED BIGR TESTS

Because the extra pellet straining (7) is deduced from the CABRI RepNa2 test data with UO₂ fuel, Zry-4 as cladding material and surface cooling by sodium, it is worthwhile to check the applicability of equation (7) to different test conditions. In the BIGR test reactor VVER fuel rods have been tested in water environment with low coolant temperature of about 25°C and with a very short pulse width of about 2.4ms [YEG 06]. The tested cladding material is E110. The tested pellet material is UO₂. This pellet is accomplished with a centre hole. The fuel rod dimensions correspond to VVER 440 and VVER 1000.

A few tests RT 8, 11 and 12 have been selected from the BIGR test program. The results are listed in table 3. Although the pellet in the BIGR test differs in design from the pellet in the CABRI test, the power pulse width in the BIGR reactor (~3ms) is much smaller than in the CABRI reactor (~10ms, ~30ms, ~75ms) and the cooling fluid is water instead of sodium as in the CABRI test loop, the prediction of the residual cladding strain by the TESP-ROD model compares well with the BIGR measurement if the power density correlation (7) is

applied. As long as no further clad straining process has influenced the BGR results, the comparison in table 3 clearly demonstrates the predictive capability of equation (7).

Table 3: Residual cladding strain in BGR tests

| Test case | Measured residual strain [%] | Predicted residual strain [%] | Burn-up [MW/kgU] | Energy Deposition [cal/g] |
|-----------|--------------------------------------|-------------------------------|------------------|---------------------------|
| RT 12 | ave. 4.35 max. 5.78 no failure | max. 5.96 | 47.3 | 198.1 |
| RT 11 | ave. 5.45 max. 8.2 failed | max. 7.67 | 47.2 | 236.5 |
| RT 8 | ave. 6.08 max. 11.1 failed | max. 6.73 | 60.0 | 201.7 |

3.1. Occurrence of DNB in the BGR test

The coolant in the BGR test section is water at atmospheric pressure. The heat flux at the cladding surface during the power pulse is large enough to change the boiling mode from sub-cooled nucleate boiling to departure from nucleate boiling (DNB). Consequently, the heat-up of the cladding increases to values which allow a creep of the cladding. Therefore, creep could be a contributor to the residual cladding strain.

Because the cooling mode DNB is not yet modeled in the TESP-ROD code, the thermal hydraulic conditions at the cladding surface have been taken from the SCANAIR code prediction, see cladding temperature in figure 5. Simultaneously the TESP-ROD prediction for fuel rod internal pressure is depicted in fig. 5 for the BGR test case RT 12, too. The pressure development is calculated on basis of the measured transient fission gas release which was determined to 22.7 % for the RT 12 test case.

According to this prediction the duration for a relevant thermal creep of the cladding is about 1.5 s, see shaded area in fig. 5. The code predictions reveal that creep is not a contributor to the residual cladding strain. In the BGR test case RT 12 the predicted residual strain is 5.78 % without DNB compared to 5.9 % with DNB. The thermal creep parameters for the E110 cladding, as it is applied in the TESP-ROD code, have been successfully validated against related cladding creep measurements.

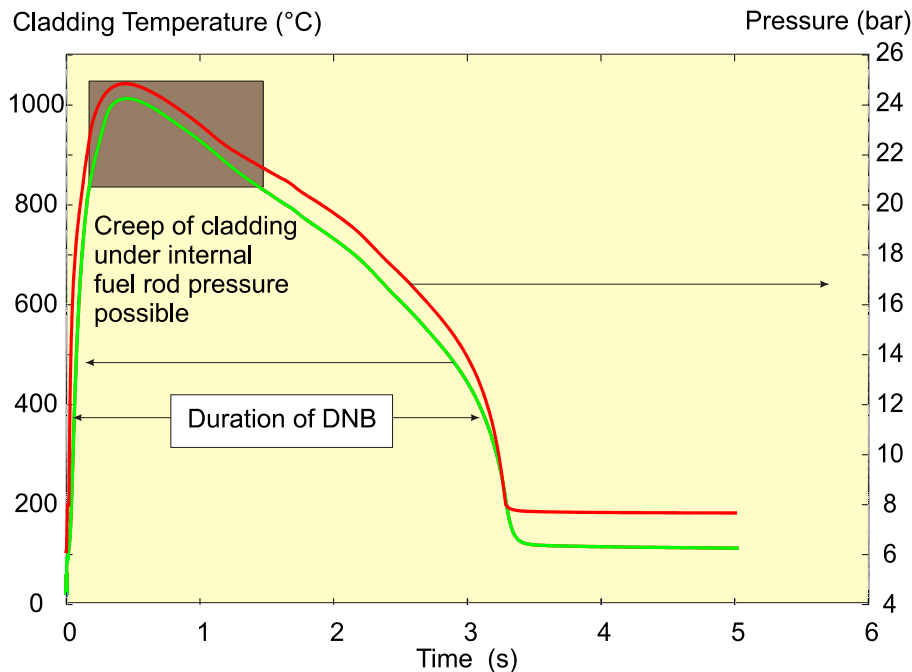


Fig. 5: Pressure and temperature development in BGR test RT 12

4. PREDICTION OF NSRR TEST LS1

Recently the post-test prediction of the LS1 test performed in the Japanese NSRR test reactor has been analysed with the TESP-ROD code. Again the boundary conditions differ from the test conditions of the CABRI and BGR in many aspects. One aspect among others is the cladding material which is Zircaloy-2 with a hydrogen content of about 300 ppm. Therefore this cladding is attributed to a ductile cladding. Although ductility of the cladding is available, the fuel rod bursts during the RIA transient. The fuel enthalpy at burst has been evaluated as 60 cal/g and the peak fuel enthalpy of 126 cal/g has been reached.

The post-test prediction with the TESP-ROD code shows a failure enthalpy of 59.4 cal/g which is quite close to the measured data. Thus the post-test prediction again appears to confirm the extra fuel strain model.

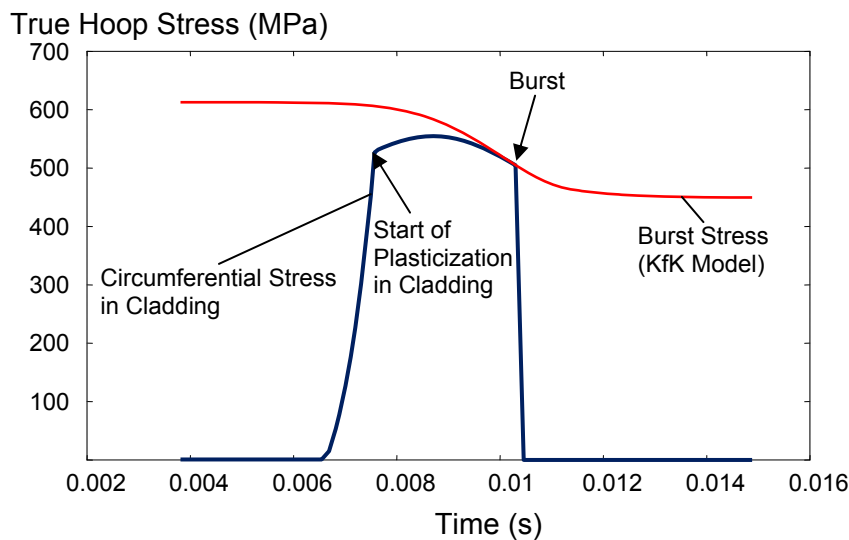


Fig. 6: Predicted circumferential stress in cladding compared with burst stress; Post-test appearance of the fuel rod LS1

The burst prediction for the LS1 test is strongly influenced by the strain hardening exponent n ($n = 0.05$) which can alter the stress/strain relation in the plastic regime. As can be seen from figure 6, there is a close competition between the decreasing burst stress on one side and the stress relaxation in the cladding due to plasticization on the other. Thus, slight modifications of the strain hardening exponent n can largely influence the timing of burst and therefore alter the burst enthalpy. Therefore, the post-test analysis of LS1 test provides only a limited validation of the fuel strain modeling.

5. CONCLUSION

The CABRI UO₂ RepNa tests, selected BIGH tests and the test LS1 from NSRR have been analyzed with the fuel rod code TESP-ROD. The TESP-ROD code applies a circumferential stress-strain relation (4) which is deduced from a 3-dimensional plasticization theory. According to this theory the ductile cladding has a yield stress to burst stress ratio which depends on the cladding geometry only. The transition from ductile to brittle cladding material is expected to be at a hydrogen up-take in the cladding of 500 ppm H. In this case the yield stress to burst stress ratio is assumed to be close to unity, see equation (5).

A simple and very efficient correlation (equation (7)) is found which determines the fuel expansion due to the expansion of micro fission gas bubbles in the fuel. It depends on the local power density of the fuel only. This model approach provides reasonable predictions for the residual cladding strain for all non-failed CABRI UO₂ tests as well as for BIGH tests. Furthermore, the enthalpy at burst measured in CABRI UO₂ tests with failed test rods as well as for the LS1 failed test rod in NSRR can precisely predicted when equation (7) is applied.

It appears that the power density correlation (7) quantifies the complex ceramic processes of both the weakening of the fuel grain due to a critical atomistic dislocation density and the subsequent expansion of the micro fission gas bubbles in a yielding fuel grain. Within the frame of data available this correlation appears to be independent from the burn-up level although the burn-up and therefore the fission gas production in UO₂ grain is a prerequisite for this expansion.

REFERENCES

- [ERB 80] Erbacher, F.; et al.: Burst Criterion of Zircaloy Fuel Cladding in a LOCA. In: ASTM 5th Intern. Conf. on Zirconium in the Nuclear Industry, Boston, Massachusetts, USA, August 4-7, 1980
- [OLA 76] Olander, D. R.: Fundamental Aspects of Nuclear Reactor Fuel Elements. TID-26711-P1, ISBN 0-87079-031-5 (v.1), Dep. of Nucl. Engineering, California, Berkeley 1976
- [PAP 03] Papin, J.; et al.: Synthesis of CABRI-RIA tests interpretation. In proceedings of Eurosafe Forum, Paris, France, November 25-26, 2003
- [PAP 06] Papin, J.; et al.: IRSN R&D studies on high burn-up fuel behaviour under RIA and LOCA conditions. In proceedings of TopFuel-2006, European Nuclear Society, pp. 274-278, Salamanca, Spain, October 22-26, 2006
- [SON 07] Sonnenburg, H.G.; et al.: Development of methods for the analysis of the fuel rod behaviour in the high burn-up regime. GRS-A-3368, 2007
- [YEG 06] Yegorova, L.; et al.: Experimental Study of Narrow Pulse Effects on the Behaviour of High Burnup Fuel Rods with Zr-1%Nb Cladding and UO₂ Fuel (VVER Type) under Reactivity-Initiated Accident Conditions: Test Conditions and Results. NUREG/IA-0213, Vol. 2, IRSN/DPAM 2005-275, NSI RRC KI 3230, 2006